Feedforward Controller With Inverse Rate-Dependent Model for Piezoelectric Actuators in Trajectory-Tracking Applications

Wei Tech Ang, *Member, IEEE*, Pradeep K. Khosla, *Fellow, IEEE*, and Cameron N. Riviere, *Member, IEEE*

***Abstract*—Effective employment of piezoelectric actuators in microscale dynamic trajectory-tracking applications is limited by two factors: 1) the intrinsic hysteretic behavior of piezoelectric ceramic and 2) structural vibration as a result of the actuator's own mass, stiffness, and damping properties. While hysteresis is rate-independent, structural vibration increases as the piezoelectric actuator is driven closer to its resonant frequency. Instead of separately modeling the two interacting dynamic effects, this work treats their combined effect phenomenologically and proposes a rate-dependent modified Prandtl–Ishlinskii operator to account for the hysteretic nonlinearity of a piezoelectric actuator at varying actuation frequency. It is shown experimentally that the relationship between the slope of the hysteretic loading curve and the rate of control input can be modeled by a linear function up to a driving frequency of 40 Hz.**

***Index Terms*—Feedforward controller, hysteresis modeling, piezoelectric actuators.**

I. Introduction

A PIEZOELECTRIC ceramic is an excellent choice as a micropositioning actuator because of its ultrafine resolution, high output force, and fast response time. However, effective employment of piezoelectric actuators in microscale dynamic trajectory-tracking applications is limited by two factors: 1) the intrinsic hysteretic behavior of piezoelectric material and 2) structural vibration as a result of the actuator's mass, stiffness, and damping properties.

The formation theory of hysteresis [1] and its complex multipath looping behavior in piezoelectric material [2] have been well documented. This highly nonlinear hysteresis complicates the control of piezoelectric actuators in high-precision applications. The maximum hysteretic error is typically about 15% in static positioning applications. Still worse, this inaccuracy is compounded with positioning errors caused by structural vibrations at higher driving frequency [3]. The resultant effect of this dynamic interaction is evident in Fig. 1, where the hysteretic loop becomes larger as the driving frequency increases.

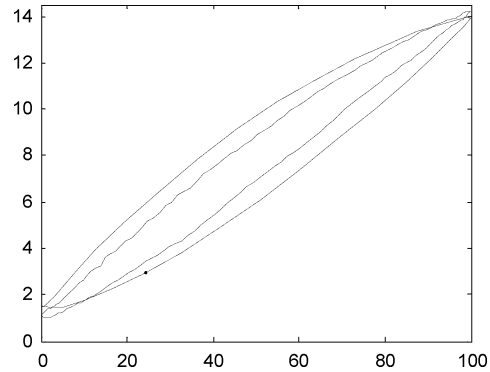

Fig. 1. Measured response of a piezoelectric actuator at two different driving frequencies. The hysteretic loop becomes larger at higher driving frequency as a result of structural vibration.

Current research in hysteresis modeling and compensation can be broadly classified into three categories: 1) electric charge control; 2) closed-loop displacement control; and 3) linear control with feedforward inverse hysteresis model. The first category exploits the fact that the relationship between the deformation of a piezoceramic and the induced charge has significantly less hysteresis than that between deformation and applied voltage [4], [5]. However, this approach requires specialized equipment to measure and amplify the induced charge, which inevitably reduces the responsiveness of the actuator. There has been little or no discussion on the effectiveness of this method in trajectory tracking at higher frequency, where the rate-dependent structural vibration comes into play.

Most commercial systems (e.g., Polytec PI, Inc., Dynamic Structures and Materials, LLC, Melles Griot, Inc., Michigan Aerospace Corporation) fall into the second category, normally using strain gauges (most common), capacitive sensors, or optical sensors as the feedback sensors. These systems can achieve nanoscale positioning precision but are generally more suitable for static positioning applications. When driven to track a 12.5-μm p-p sinusoid at 10 Hz, the Polytec PI NanoCube exhibits a system response that resembles that of a low-pass filter, i.e., diminishing magnitude gain with frequency increment and with the response phase lagging the control input. The effect of hysteresis remains evident and the closed-loop controller manages tracking of maximum error and rms error of 7.8 (62.4% of p-p amplitude) and 3.1 μm (24.8%), respectively.

Other proposed closed-loop schemes to treat hysteresis include linearizing the hysteretic nonlinearity [6], using adaptive control with an approximate model of the hysteresis [7],

Manuscript received January 20, 2006; revised April 1, 2006. Recommended by Technical Editor N. Jalili. This work was supported in part by the National Institutes of Health under Grant R01 EB000526 and in part by the National Science Foundation under Grant EEC-9731748.

W. T. Ang is with the School of Mechanical and Aerospace Engineering, Nanyang Technological University, Singapore 639798 (e-mail: wtang@ntu.edu.sg).

P. K. Khosla is with the Department of Electrical Engineering and the Robotics Institute, Carnegie Mellon University, Pittsburgh, PA 15213 USA (e-mail: pkk@ece.cmu.edu).

C. N. Riviere is with the Robotics Institute, Carnegie Mellon University, Pittsburgh, PA 15213 USA (e-mail: camr@ri.cmu.edu).

Digital Object Identifier 10.1109/TMECH.2006.892824

training a neural network to learn the nonlinearity [8], or a combination of neural network with adaptive control [9]. These control schemes are not suitable for more dynamic tracking scenarios, because of the intrinsic stability problem with high feedback gains [10], [11].

The main idea of the third category is to obtain a mathematical model that closely describes the complex hysteretic behavior and then, to implement an inverse feedforward controller based on the inverse hysteresis model to linearize the actuator response.

Among the proposed hysteresis models, e.g., the Maxwell's slip model [12], the Duhem model [13], and polynomial approximation [3], [14], the Preisach model [15]–[17] and its variations [18] are by far the most well known and widely used in both closed-loop [16], [17] and open-loop [18] systems. However, most of these methods do not work for nonstationary sinusoids because of the intrinsic properties of the classical Preisach model [16]. Another important subclass of the Preisach model is the Prandtl–Ishlinskii (PI) model [19]–[21]. The main advantages of the PI operator over the classical Preisach operator are that it is simpler and its inverse can be computed analytically, thus making it more attractive for real-time applications [19].

One convenient approach to reduce the position errors caused by structural vibration is to keep operating frequency further from the actuator's resonant frequency by using actuators with either larger mass or shorter piezotubes [22]. Feedback control schemes have also shown some improvement in the dynamic response, but the tradeoff would be the inevitable system instability at high feedback gains [10], [11].

The dynamic interaction between the structural vibration and hysteresis, as appeared in some literatures, is due to the rate-dependence property of the piezoelectric ceramic hysteresis [23], [24]. On the other hand, Croft and Devasia [3] treat the phenomenon as a superimposition of rate-independent hysteresis and rate-dependent piezo-system dynamics. An open-loop control scheme is implemented with feedforward inverse hysteresis model and inverse piezodynamic model. Hysteresis is modeled by a third-order polynomial while the piezodynamics up to 1 kHz is modeled by a fourth-order transfer function with the aid of a dynamic signal analyzer. Instead of separately modeling the two interacting dynamic effects, we treat their combined effect phenomenologically and propose a rate-dependent modified PI operator to account for the hysteretic nonlinearity and errors caused by structural vibrations of a piezoelectric actuator at varying actuation frequency [25]. We show experimentally that the slope of the hysteresis loading curve is linearly dependent on the rate of the control input. We implement an open-loop inverse feedforward controller based on the rate-dependent modified PI hysteresis model and compare the experimental results with the rate-independent case. A discussion on the significance of the result and the model limitations is also presented.

While a well-implemented feedback controller may have a better tracking accuracy than a feedforward open-loop controller, it introduces a phase-lag between the driving function and the plant response. In real-time trajectory-tracking applications, such as active noise or vibration compensation, this inevitable phase shift would cause a larger tracking error than that resulted from feedforward model inaccuracies, especially at higher frequencies where the phase-lag is more significant.

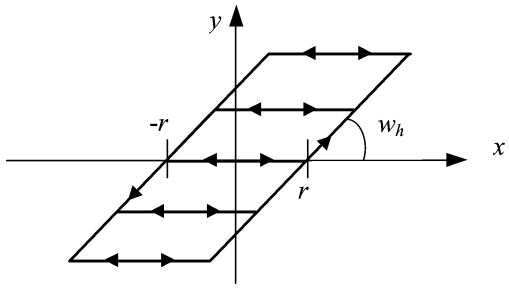

Fig. 2. Rate-independent generalized backlash operator is characterized by the threshold or backlash magnitude r, and the weight or backlash operator gain w_h.

II. PI Hysteresis Model

A. PI Operator

The elementary operator in the PI hysteresis model is a rate-independent backlash operator. It is commonly used in the modeling of backlash between gears with one degree of freedom. A backlash operator is defined by

$$\begin{aligned} y(t) &= H_r[x, y_0](t) \\ &= \max\{x(t) - r, \min\{x(t) + r, y(t - T)\}\} \end{aligned} \tag{1}$$

where x is the control input, y is the actuator response, r is the control input threshold value or the magnitude of the backlash, and T is the sampling period. The initial consistency condition of (1) is given by

$$y(0) = \max\{x(0) - r, \min\{x(0) + r, y_0)\}\} \tag{2}$$

where $y_0 \in \Re$, and is usually but not necessarily initialized to 0. Multiplying the backlash operator H by a weight value w_h, we have the generalized backlash operator

$$y(t) = w_h H_r\,[x, y_0]\,(t). \tag{3}$$

The weight w_h defines the gain of the backlash operator ($w_h = y/x$; hence, $w_h = 1$ represents a 45° slope) and may be viewed as the gear ratio in an analogy of mechanical play between gears, as shown in Fig. 2.

Complex hysteretic nonlinearity can be modeled by a linearly weighted superposition of many backlash operators with different threshold and weight values

$$y(t) = \vec{w}_h^T \vec{H}_r\,[x, \vec{y}_0](t) \tag{4}$$

with weight vector $\vec{w}_h^T = [w_{h0} \ldots w_{hn}]$ and $\vec{H}_r\,[x, \vec{y}_0](t) = [H_{r0}[x, y_{00}](t) \ldots H_{rn}[x, y_{0n}](t)]^T$ with the threshold vector $\vec{r} = [r_0 \ldots r_n]^T$ where $0 = r_0 < \ldots < r_n$, and the initial state vector $\vec{y}_0 = [y_{00} \ldots y_{0n}]^T$. The control input threshold values $\vec{r}$ are usually, but not necessarily, chosen to be equal intervals. If the hysteretic actuator starts in its deenergized state, then $\vec{y}_0 = \vec{0}_{n\times 1}$.

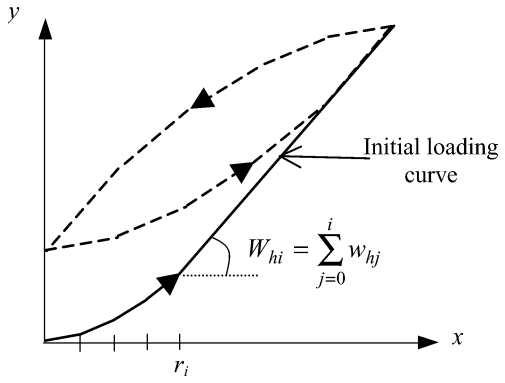

Fig. 3. PI hysteresis model with $n = 4$. The hysteresis model is characterized by the initial loading curve. The piecewise linear curve is defined by the equally spaced threshold values $\vec{r}$ and the sum of the weight values $\vec{w}_h$.

Equation (4) is the PI hysteresis operator in its threshold discrete form. The hysteresis model formed by the PI operator is characterized by the initial loading curve (see Fig. 3). It is a special branch traversed by (4) when driven by a monotonically increasing control input with its state initialized to zero (i.e., $y(0) = 0$). The initial loading curve is defined by the weight values $\vec{w}_h$ and threshold values $\vec{r}$

$$\varphi(r) = \sum_{j=0}^{i} w_{hj}(r - r_j), \qquad r_i \le r < r_{i+1}; \quad i = 0, \ldots, n. \tag{5}$$

The slope of the piecewise-linear curve at interval i is defined by W_{hi}, the sum of the weights up to i, as

$$W_{hi} = \frac{d}{dr}\varphi(r) = \sum_{j=0}^{i} w_{hj}. \tag{6}$$

The subsequent trajectory of the PI operator beyond the initial loading curve with nonnegative control input is shown as the dotted loop in Fig. 3. The hysteresis loop formed by the PI operator does not return to zero with the control input. This behavior of the PI operator closely resembles the hysteresis of a piezoelectric actuator.

The backlash operators cause each of the piecewise linear segments to have a threshold width of $2r$ beyond the initial loading curve. As such, there is no need to define any backlash operator beyond the midpoint of the control input range, i.e., $r_n \le 1/2 \max\{\text{control input}\}$. This also implies that the backlash operators have descending importance from the first to the last, since the first operator is always used and the subsequent operators are only used when the control inputs go beyond their respective threshold values r_i. Moreover, observations from the piezoelectric hysteretic curves suggest that more drastic changes in the slope occur after the turning points, i.e., in the region of the first few backlash operators. To strike a balance between model accuracy and complexity, we propose to importance-sample the threshold intervals $\vec{r}$, i.e., to have finer intervals for the first few backlash operators and increasing intervals for the subsequent ones. The tradeoffs of choosing different threshold intervals will be discussed further in Section VI.

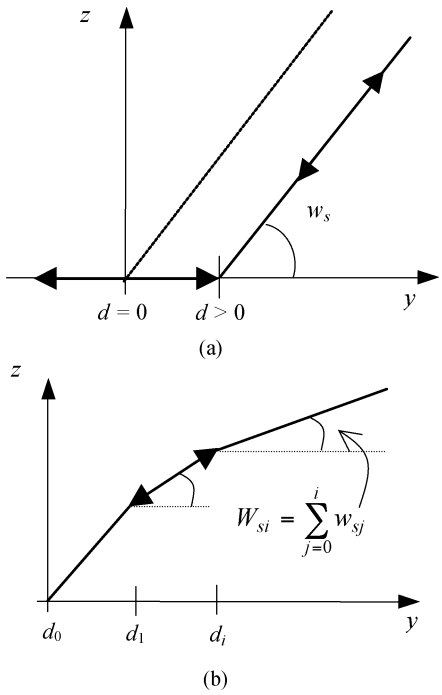

Fig. 4. (a) One-sided dead-zone operator is characterized by the threshold d, and the gain w_s. (b) Saturation operator with $m = 2$. The slope of the piecewise linear curve at interval i, W_{si} is defined by the sum of the weights up to i.

B. Modified PI Operator

The PI operator inherits the symmetry property of the backlash operator at about the center point of the loop formed by the operator. The fact that most real actuator hysteretic loops are not symmetric weakens the model accuracy of the PI operator. To overcome this overly restrictive property, a saturation operator is combined in series with the hysteresis operator. A saturation operator is a weighted linear superposition of linear-stop or one-sided dead-zone operators. A dead-zone operator is a nonconvex, asymmetrical, memory-free nonlinear operator (Fig. 4).

A one-sided dead-zone operator and a saturation operator are given by

$$S_d[y](t) = \begin{cases} \max\{y(t) - d, 0\}, & d > 0 \\ y(t), & d = 0 \end{cases} \tag{7}$$

$$z(t) = \vec{w}_s^{\,T} \vec{S}_d\,[y](t) \tag{8}$$

where y is the output of the hysteresis operator, z is the actuator response, $\vec{w}_s^{\,T} = [w_{s0} \ldots w_{sm}]$ is the weight vector, $\vec{S}_d\,[y](t) = [S_{d0}[y](t) \ldots S_{dm}[y](t)]^T$ with the threshold vector $\vec{d} = (d_0 \ldots d_m)^T$ where $0 = d_0 < d_1 < \ldots < d_m$. For convenience, intervals of $\vec{d}$ between d_0 and d_m need not be equal. Good selection of $\vec{d}$ depends on the shape of the hysteresis loop, and typically involves some trials and errors.

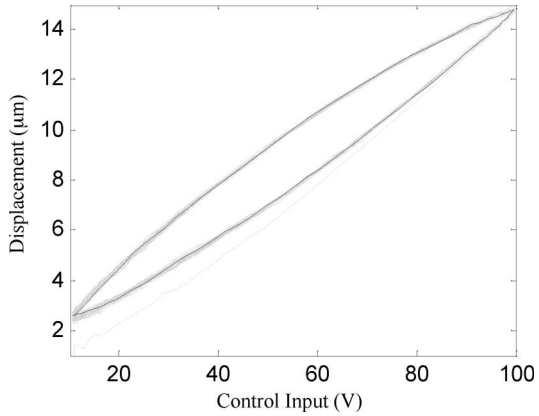

Fig. 5. Lighter solid lines are the measured piezoelectric actuator response to a 10-Hz, 12.5-μm p-p sinusoidal control input. The dark dotted line is the identified modified PI hysteresis model with ten backlash operators ($n = 9$) and four dead-zone operators ($m = 3$).

The modified PI operator is thus

$$z(t) = \Gamma[x](t) = \vec{w}_s^T \vec{S}_d \left[\vec{w}_h^T \vec{H}_r \left[x, \vec{y}_0\right]\right](t). \tag{9}$$

C. Parameter Identification

To find the hysteresis model parameters, we first have to measure experimentally the responses of the piezoelectric actuator to periodic control inputs. A good set of identification data is one that covers the entire operational actuation range of the piezoelectric actuator at the nominal operating frequency. Next, we decide the order of the PI operator (n) and the saturation operator (m), and set the threshold values $\vec{r}$ and $\vec{d}$ as described in Section II-B. The weight parameters $\vec{w}_h$ and $\vec{w}_s$ are found by performing a least-squares fit of (9) to the measured actuator response, minimizing the error equation

$$E[x, z](\vec{w}_h, \vec{w}_s, t) = \vec{w}_s^T \vec{S}_d \left[\vec{w}_h^T \vec{H}_r \left[x, \vec{y}_0\right]\right](t) - z(t). \tag{10}$$

Fig. 5 shows superposition of the identified modified PI hysteresis model on the measured piezoelectric actuator response, subjected to a sinusoidal control input.

D. Inverse Modified PI Operator

The key idea of an inverse feedforward controller is to cascade the inverse hysteresis operator Γ^{-1} with the actual hysteresis, which is represented by the hysteresis operator Γ, to obtain an identity mapping between the desired actuator output $\hat{z}(t)$ and actuator response $z(t)$ as

$$z(t) = \Gamma\left[\Gamma^{-1}[\hat{z}]\right](t) = I[\hat{z}](t) = \hat{z}(t). \tag{11}$$

The operation of the inverse feedforward controller is depicted in Fig. 6.

The inverse of a PI operator is also of the PI type. The inverse PI operator is given by

$$\Gamma^{-1}[\hat{z}](t) = \vec{w}_h'^T \vec{H}_{r'} \left[\vec{w}_s'^T \vec{S}_{d'} \left[\hat{z}\right], \vec{y}_0'\right](t) \tag{12}$$

where the inverse modified PI parameters can be found by

$$w'_{h0} = \frac{1}{w_{h0}} \quad w'_{hi} = \frac{-w_{hi}}{(\sum_{j=0}^{i} w_{hj})(\sum_{j=0}^{i-1} w_{hj})}, \quad i = 1 \ldots n$$

$$r'_i = \sum_{j=0}^{i} w_{hj}(r_i - r_j) \quad y'_{0i} = \sum_{j=0}^{i} w_{hj} y_{0i} + \sum_{j=i+1}^{n} w_{hj} y_{0j}, \qquad i = 1 \ldots n \tag{13}$$

$$w'_{s0} = \frac{1}{w_{s0}} \quad w'_{si} = \frac{-w_{si}}{(\sum_{j=0}^{i} w_{sj})(\sum_{j=0}^{i-1} w_{sj})}, \quad i = 1 \ldots m$$

$$d'_i = \sum_{j=0}^{i} w_{sj}(d_i - d_j), \qquad i = 0 \ldots m. \tag{14}$$

Graphically, to compute the inverse is to find the reflection of the resultant hysteresis looping curves about the 45° line as shown in Fig. 7.

III. Rate-Dependent PI Hysteresis Model

A. Rate-Dependent Hysteresis Slope

We propose in this section, an extension to the modified PI operator to also model the rate-dependent characteristics of the piezoelectric hysteresis.

One of the advantages of the PI hysteresis model is that it is purely phenomenological; there are no direct relationships between the modeling parameters and the physics of the hysteresis. Therefore, we model the rate-dependent hysteresis with reference only to the experimental observations. While the rate dependence of hysteresis is evident from Fig. 1, the sensitivity of actuator saturation to the actuation rate is not apparent. Hence, we assume that saturation is not rate dependent and hold the saturation weights $\vec{w}_s$ as well as the threshold values $\vec{r}$ and $\vec{d}$ constant while attempting to construct a relationship between hysteresis and the rate of actuation $\dot{x}(t)$. We model the slope of the hysteresis curve (i.e., sum of the PI weights) at time t as the sum of the referenced hysteresis slope and a rate-dependent function as

$$W_{hi}(\dot{x}(t)) = \hat{W}_{hi} + f(\dot{x}(t)), \qquad i = 1 \ldots n \tag{15}$$

where

$$\dot{x}(t) = \frac{x(t) - x(t - T)}{T}, \qquad \dot{x}(0) = 0. \tag{16}$$

Equation (15) will be reduced to the referenced hysteresis slope $\hat{W}_{hi}$ or to the rate-independent case, if the rate-dependent term is zero.

B. Rate-Dependent Model Identification

The response of a piezoelectric actuator subjected to periodic constant-rate or sawtooth control inputs is first measured. Measurements are made over a frequency band, whose equivalent rate values cover the entire operational range of the actuation rates. For example, in an application tracking sinusoids of up

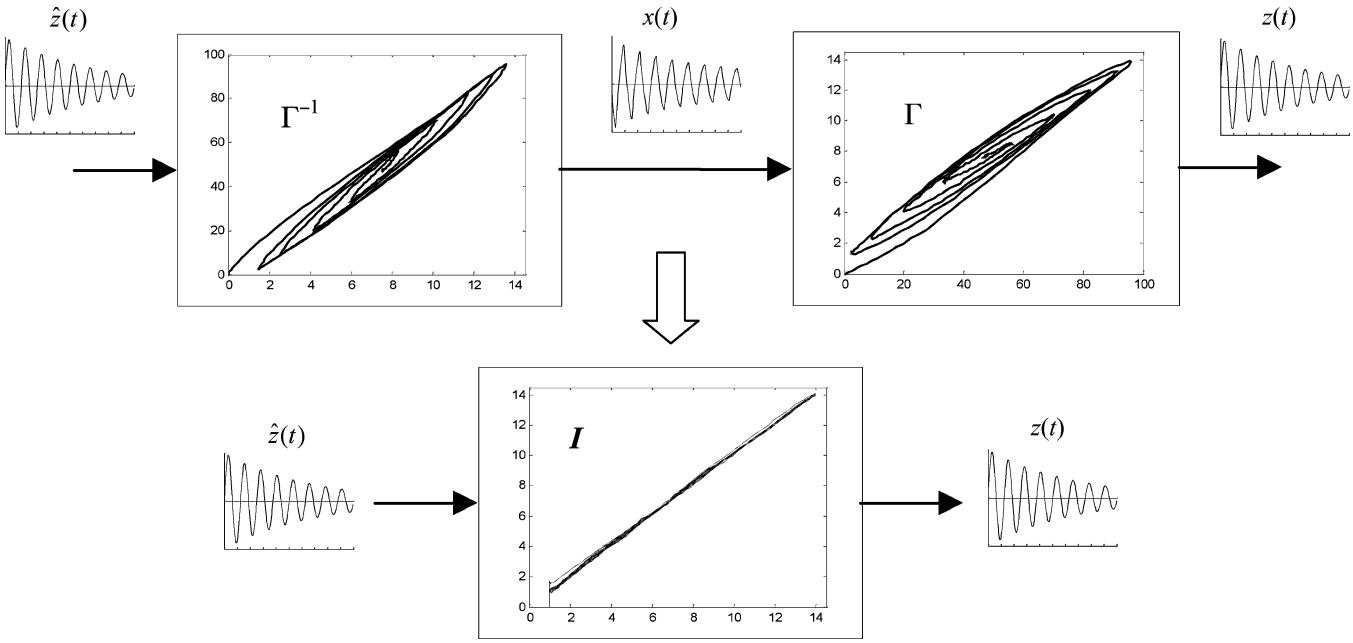

Fig. 6. Inverse feedforward controller. Given a desired periodic actuator output $\hat{z}(t)$, the inverse modified PI operator Γ^{-1} transforms it into a control input $x(t)$, which produces a response $z(t)$ in the hysteretic system that closely resembles $\hat{z}(t)$. This produces an equivalent control system with identity mapping between the desired output and the actual actuator response.

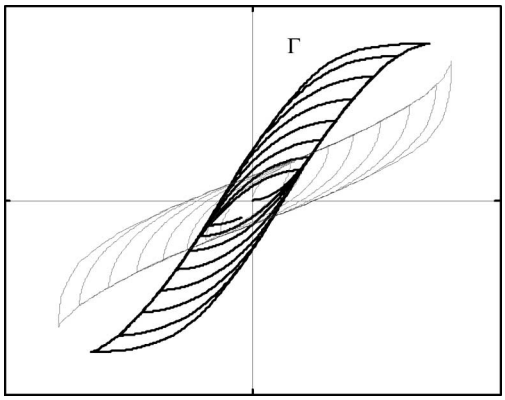

Fig. 7. Darker thick line is the modified PI hysteresis model Γ. The inverse modified PI hysteresis model Γ^{-1}, represented by the lighter thin line, is the mirror image of the hysteresis model about the 45° line.

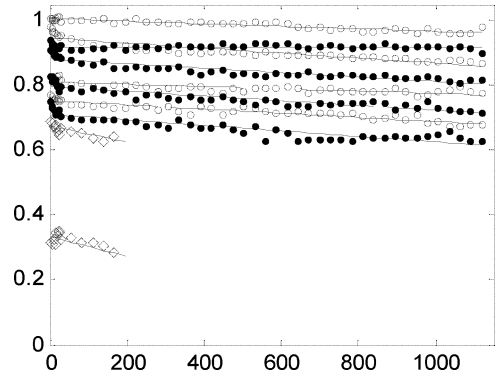

Fig. 8. Plot of the hysteresis slopes W_{hi}, $i = 1$ to 9, versus actuation rate $\dot{x}(t)$. Since the actuation rate is always slow at the turning points of a sinusoid, the first two sums of weights W_{h0} and W_{h1} are modeled up to 200 μm/s.

to 12.5-μm p-p in the band of 1–19 Hz, the operational range of the actuation rate is from 0 to 746 μm/s, which corresponds to the rate of 12.5-μm p-p sawtooth waveforms of up to about 60 Hz. PI parameter identification is then performed on each set of measured actuator responses.

The sum of the hysteresis weights W_{hi}, $i = 0 \ldots n$, of each identification is plotted against the actuation rate $\dot{x}(t)$ in Fig. 8.

We observe that the hysteresis slope of the piezoelectric actuator varies linearly with the actuation rate. Thus the rate-dependent hysteresis slope model would be

$$W_{hi}(\dot{x}(t)) = \hat{W}_{hi} + c_i \dot{x}(t), \qquad i = 0 \ldots n \tag{17}$$

where c_i is the slope of the best fit line through the W_{hi}, and the referenced slope W_{hi} is the intercept of the best fit line with the vertical W_h axis or the slope at zero actuation. The individual rate-dependent hysteresis weight values can be calculated from

$$w_{hi}(\dot{x}(t)) = W_{hi}(\dot{x}(t)) - W_{h(i-1)}(\dot{x}(t)), \qquad i = 1 \ldots n$$
$$w_{h0}(\dot{x}(t)) = W_{h0}(\dot{x}(t)). \tag{18}$$

C. Rate-Dependent Modified PI Operator

The rate-dependent modified PI operator is defined by

$$z(t) = \Gamma[x, \dot{x}](t) = \vec{w}_s^T \vec{S}_d \left[\vec{w}_h^T \ (\dot{x}) \ \vec{H}_r \ [x, \vec{y}_0] \right](t). \tag{19}$$

The inverse rate-dependent modified PI operator is also of the PI type

$$\Gamma^{-1}[\hat{z}](t) = \vec{w}_h'^T \ (\dot{x}) \ \vec{H}_{r'} \left[\vec{w}_s'^T \vec{S}_{d'} \ [\hat{z}], \vec{y}'_0 \right](t). \tag{20}$$

The inverse rate-dependent parameters can be found by (13), replacing $\vec{w}_h$ with the rate-dependent $\vec{w}_h\ (\dot{x})$, as (21), shown at the bottom of the page.

IV. Model Identification Experiments

Open-loop controllers with feedforward inverse rate-independent and rate-dependent modified PI models are to be implemented on a P-885.50 piezoelectric stack actuator (Polytec PI, Inc., Karlsruhe, Germany), which measures 5 mm $\times$ 5 mm $\times$ 18 mm. The piezoelectric actuator is controlled by a Pentium computer via a digital-to-analog converter (DAC) sampled at 1 kHz and a power amplifier with 20X gain. The displacement of the piezoelectric actuator is measured by an infrared interferometer (Philtec, Inc., Model D63) sampled and recorded at 1 kHz via an analog-to-digital conveter (ADC). The measurement noise of the interferometer is 0.03-μm rms.

The modeling experiments are performed under no load or free actuating condition, i.e., only the dynamics of the piezoelectric actuator is modeled. It should be noted that when the actuators are to be used in a positioning system, modeling should be performed as a complete piezosystem with the actuation mechanism and load, in order to capture the full system dynamics. The vicinity of the experiment setup is well ventilated and is regulated at 21°C.

The rate-independent model uses a PI operator of order 9 ($n = 9$, i.e., ten backlash operators) and a saturation operator of order 3 ($m = 3$, i.e., four dead-zone operators). These parameters are selected by an iterative process, whereby the order of the operators is systematically increased until the modeling performance improvement becomes insignificant ($< 1\%$ in our case). The PI thresholds $\vec{r}$ are selected to be multiples of five from 0 to 45, and the saturation thresholds are $\vec{d} = [0\,63.3\,74.8\,87.3]^T$. The identification of the PI and saturation weights is based on the measured response of the piezoelectric actuators to a 10-Hz, 12.5-μm p-p sinusoidal control input. A 5-s motion sequence or 5000 data points are used for the identification. There is no compelling reason for choice of 10 Hz as the base frequency, except to be consistent with the operating condition of the application to be presented in Section VII.

The rate-dependent model uses the same order of modified PI operator and saturation operator, i.e., $n = 9$ and $m = 3$. Importance-sampled PI thresholds are used, with $\vec{r} = [0\,4\,8\,12\,16\,20\,25\,31\,38\,45]^T$. Identification of PI parameters is performed on the measured actuator response subjected to 12.5-μm p-p sawtooth control input at intervals of 0.1 Hz in the band of 0.1–5.0 Hz, and at intervals of 1 Hz in the band of 5–40 Hz. Since we assume the actuator saturation is rate-independent, the same saturation thresholds and weights of the rate-independent model are used.

TABLE I
Measured Performance of the Rate-Independent and Rate-Dependent Inverse Feedforward Controllers in Tracking 12.5-μm p-p Stationary Sinusoids

	Without Model		Rate-independent		Rate-dependent	
Freq. (Hz)	rmse (μm)	max ε (μm)	rmse (μm)	max ε (μm)	rmse (μm)	max ε (μm)
1	1.13	2.11	0.25	0.63	0.21	0.57
4	1.12	2.07	0.19	0.67	0.16	0.46
7	1.23	2.24	0.18	0.52	0.16	0.50
10	1.19	2.26	0.14	0.46	0.17	0.47
13	1.21	2.31	0.19	0.53	0.17	0.55
16	1.30	2.49	0.27	0.59	0.17	0.53
19	1.37	2.61	0.34	0.70	0.18	0.59
Mean ± σ	1.22 ± 0 09	2.30 ± 0.19	0.23 ± 0.07	0.59 ± 0.8	0.18 ± 0.02	0.52 ±0.05

Maximum errors and rms errors are the mean results over a set of three 5-s (5000 data points) experiments.

V. Motion Tracking Experiments

Two motion tracking experiments are performed with the same setup and under the same conditions as described in Section IV. The first experiment compares the performance of the rate-independent and rate-dependent modified PI models based open-loop feedforward controllers in tracking a 10-Hz, 12.5-μm p-p stationary sinusoid. The experiment is repeated to track 12.5-μm p-p stationary sinusoids at 1, 4, 7, 13, 16, and 19 Hz. The tracking rms error and maximum error of the controllers at each frequency is summarized in Table I and plotted in Fig. 9. Fig. 10(a) plots the hysteretic response of the piezoelectric actuator with a proportional controller. Fig. 10(b)–(c) show the tracking results of the rate-independent and rate-dependent inverse feedforward controllers.

The second experiment compares the performance of the controllers in tracking a multifrequency, nonstationary, and dynamic motion profile. The motion profile is made up of superimposed modulated 1-, 10-, and 19-Hz sinusoids with time-varying

$$
\begin{aligned}
w'_{h0}\left(\dot{x}(t)\right) &= \frac{1}{w_{h0}\left(\dot{x}(t)\right)}; \quad w'_{hi}\left(\dot{x}(t)\right) = \frac{-w_{hi}\left(\dot{x}(t)\right)}{W_{hi}\left(\dot{x}(t)\right) W_{h(i-1)}\left(\dot{x}(t)\right)}, \qquad i = 1 \ldots n \\
r'_i &= \sum_{j=0}^{i} w_{hj}\left(\dot{x}(t)\right)\left(r_i - r_j\right), \qquad i = 0 \ldots n \\
y'_{0i} &= \sum_{j=0}^{i} w_{hj}\left(\dot{x}(t)\right) y_{0i} + \sum_{j=i+1}^{n} w_{hj}\left(\dot{x}(t)\right) y_{0j}, \qquad i = 0 \ldots n.
\end{aligned} \tag{21}
$$

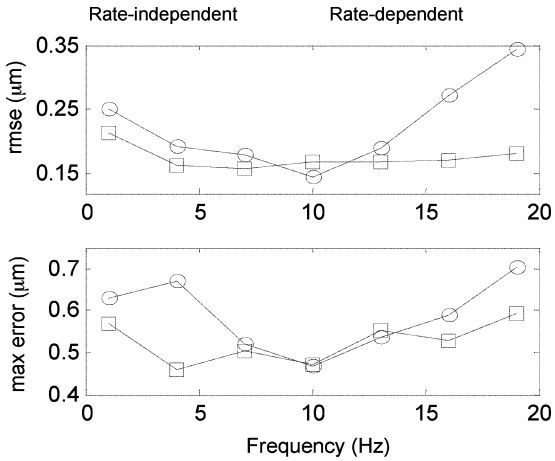

Fig. 9. Maximum errors and rms errors of the rate-independent and rate-dependent controllers in tracking 12.5-μm p-p stationary sinusoids at different frequencies. The rate-independent controller is based on the modified PI hysteresis model identified at the same 10-Hz, 12.5-μm p-p sinusoid.

amplitudes. The graphical and numerical results are shown in Fig. 11 and Table II, respectively.

VI. Discussion

In the first experiment, tracking 12.5-μm p-p stationary sinusoids, both the rate-independent and rate-dependent controllers significantly reduced the tracking error due to the hysteretic nonlinearity of the piezoelectric actuator. On an average, the rate-independent controller reduces the tracking rms error and maximum error by 81.7% and 74.4%, respectively in the band of 1–19 Hz. The best performance occurs at 10 Hz, in which its modified PI hysteresis model parameters are identified. The tracking accuracy deteriorates as the tracking frequency deviates from 10 Hz. The rate-dependent controller outperforms its rate-independent counterpart with tracking rms error and maximum error reduction of 85.6% and 77.2%, respectively. The tracking accuracy remains consistent across the entire 1–19-Hz band. At 19 Hz, the tracking rms error of the rate-independent controller is almost double that of the rate-dependent controller, and will continue to worsen as the frequency increases. Maximum tracking errors for both controllers occur in the transient phase at the beginning of the test.

In the second experiment, tracking a multifrequency (1, 10, and 19 Hz) nonstationary motion profile, similar results are observed. Both the controllers continue to perform well, the rate-independent controller reducing the rms error and maximum error by 69.6% and 53.4%, and the rate-dependent controller doing noticeably better at 85.3% and 69.1%, respectively.

The rate-dependent controller registers a tracking rms error less than half of that of the rate-independent controller. Maximum tracking errors for both the controllers again occur in the transient phase at the beginning of the test. This could be the reason why the improvement in maximum error with the rate-dependent controller is not as large as the improvement in rms error.

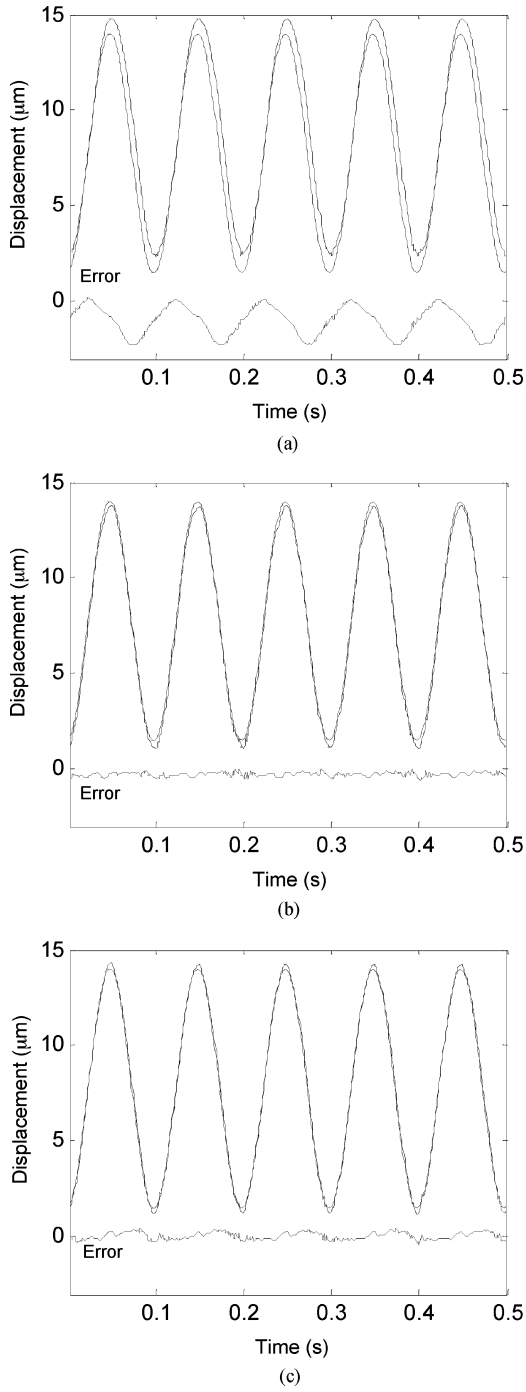

Fig. 10. Experimental open-loop tracking results of stationary 12.5-μm p-p sinusoids at 10 Hz. The rate-independent controller is based on the modified PI hysteresis model identified at the same 10-Hz, 12.5-μm p-p sinusoid. (a) Without controller. (b) Rate-independent controller. (c) Rate-dependent controller.

One limitation of all PI-type hysteresis models is that singularity occurs when the first PI weight w_{h0} is zero; the inverse weight w'_{h0} then becomes undefined [refer to (13) and (21)]. Also, when the slope is negative, the inverse hysteresis loading curve violates the fundamental assumption that it should be monotonically increasing, and since the one-to-one mapping relationship between the direct and the inverse model is lost, the PI operator breaks down.

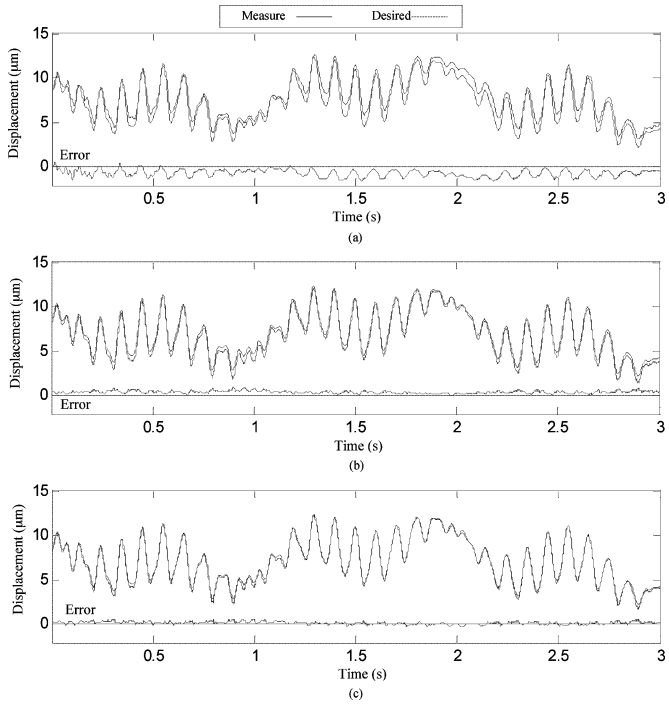

Fig. 11. Experimental open-loop tracking results of a multifrequency, nonstationary, dynamic motion profile. The motion profile is made up of superimposed modulated 1-, 10-, and 19-Hz sinusoids with time-varying amplitudes. The rate-independent controller is based on the modified PI hysteresis model identified at the same 10-Hz, 12.5-μm p-p sinusoid. Transient error is observed for the rate-independent controller in the first 2 s. (a) Without compensation. (b) Rate-independent controller. (c) Rate-dependent controller.

TABLE II
MEASURED PERFORMANCE OF THE RATE-INDEPENDENT AND RATE-DEPENDENT INVERSE FEEDFORWARD CONTROLLERS IN TRACKING MULTIFREQUENCY (1-, 10-, AND 19-HZ) NONSTATIONARY SIGNALS

	Without model	Rate-independent	Rate-dependent
rmse $\pm \sigma$ (μm)	1.02 ± 0.07	0.31 ± 0.03	0.15 ± 0.003
$\frac{\text{rmse}}{\text{p - p amplitude}}$ (%)	9.2	2.8	1.4
max error $\pm \sigma$ (μm)	1.91 ± 0.08	0.89 ± 0.04	0.59 ± 0.06
$\frac{\text{max error}}{\text{p - p amplitude}}$ (%)	17.3	8.0	5.3

Maximum errors and rms errors are the mean results over a set of three 5-s (5000 data points) experiments.

Singularities occur more easily at higher frequency, where the hysteresis loop gets larger and is more rounded at the turning points. For a given piezoelectric actuator, the singular frequency of a PI model depends on the choice of the thresholds $\vec{r}$. Choosing a larger first interval r_1 can raise the singularity frequency, but the tradeoff would be poorer modeling accuracy at the turning points. The singularity of our implementation for tracking 12.5-μm p-p sinusoids occurs at around 40 Hz.

Despite this shortcoming, for applications that do not require very high actuation frequency, the proposed method offers an alternative to [3] to account for hysteresis and structural vibrations of piezoelectric actuators with a simpler experimental setup, a less complex model, and comparable performance that is well suited for real-time implementation. Future work will focus on overcoming the intrinsic singularity imposed by the PI operator to cater to higher actuation frequency.

Creep is not modeled here because its effect is negligible for periodic excitation with frequency higher than 1 Hz. If quasistatic tracking is desired, since the rate-dependent model and its inverse are also of the PI type, the creep model proposed by Krejci and Kuhnen [20] can be incorporated.

VII. CONCLUSION

Errors caused by the dynamic interaction between hysteretic nonlinearity and structural vibrations of a piezoelectric actuator limit its effectiveness in higher frequency dynamic trajectory-tracking applications. We have presented a rate-dependent modified PI model to account for this dynamic behavior. The proposed method uses a linear function to model the relationship between the slopes of the hysteretic loading curve and the actuation rate. An open-loop inverse feedforward controller, based on the rate-dependent modified PI model, is implemented on a piezoelectric actuator. Experimental results have shown that the proposed rate-dependent controller consistently outperforms its rate-independent counterpart in tracking dynamic motion profiles.

REFERENCES

[1] P. Chen and S. Montgomery, "A macroscopic theory for the existence of the hysteresis and butterfly loops in ferroelectricity," *Ferroelectrics*, vol. 23, pp. 199–207, 1980.
[2] M. A. Krasnosel' skii and A. V. Pokrovskii, *Systems with Hysteresis,* New York: Springer-Verlag, 1989.
[3] D. Croft and S. Devasia, "Hysteresis and vibration compensation for piezoactuators," *J. Guid., Control Dyn.*, vol. 21, no. 5, pp. 710–717, 1998.
[4] C. Newcomb and I. Filnn, "Improving linearity of piezoelectric ceramic actuators," *Electron. Lett.*, vol. 18, no. 11, pp. 442–444, May 1982.
[5] K. Furutani, M. Urushibata, and N. Mohri, "Displacement control of piezoelectric element by feedback of induced charge," *Nanotechnology*, vol. 9, pp. 93–98, 1998.
[6] C. Jan and C.-L. Hwang, "Robust control design for a piezoelectric actuator system with dominant hysteresis," in *Proc. 26th Annu. Conf. IEEE Ind. Electron. Soc.*, Nagoya, Japan, vol. 3, Oct. 2000, pp. 1515–1520.
[7] G. Tao and P. V. Kokotovic, "Adaptive control of plants with unknown hystereses," *IEEE Trans. Autom. Control*, vol. 40, no. 2, pp. 200–212, Feb. 1995.
[8] S.-S. Ku, U. Pinsopon, S. Cetinkunt, and S. Nakjima, "Design, fabrication, and real-time neural network of a three-degrees-of-freedom nanopositioner," *IEEE/ASME Trans. Mechatronics*, vol. 5, no. 3, pp. 273–280, Sep. 2000.
[9] C.-L. Hwang and C. Jan, "A reinforcement discrete neuro-adaptive control for unknown piezoelectric actuator systems with dominant hysteresis," *IEEE Trans. Neural Netw.*, vol. 14, no. 1, pp. 66–78, Jan. 2003.
[10] J. A. Main and E. Garcia, "Piezoelectric stack actuators and control system design: Strategies and pitfalls," *J. Guid., Control Dyn.*, vol. 20, no. 3, pp. 479–485, 1997.
[11] N. Tamer and M. Dahleh, "Feedback control of piezoelectric tube scanners," in *Proc. 33rd IEEE Conf. Decision Control*, Lake Buena Vista, FL, Dec. 1994, vol. 2, pp. 1826–1831.
[12] M. Goldfarb and N. Celanovic, "Modeling piezoelectric stack actuators for control of micromanipulation," *IEEE Control Syst. Mag.*, vol. 17, no. 3, pp. 69–79, Jun. 1997.
[13] Y. Stepanenko and C.-Y. Su, "Intelligent control of piezoelectric actuators," in *Proc. IEEE Conf. Decision Control*, Tampa, FL, Dec. 1998, pp. 4234–4239.

[14] S. Chonan, Z. Jiang, and T. Yamamoto, "Nonlinear hysteresis compensation of piezoelectric ceramic actuators," *J. Intell. Mater. Syst. Struct.*, vol. 7, no. 2, pp. 150–156, 1996.
[15] D. Huges and J. T. Wen, "Preisach modeling of piezoceramic and shape memory alloy hysteresis," in *Proc. 4th IEEE Conf. Control Appl.*, Albany, NY, Sep.1995, pp. 1086–1091.
[16] P. Ge and M. Jouaneh, "Tracking control of a piezoceramic actuator," *IEEE Trans. Control Syst. Technol.*, vol. 4, no. 3, pp. 209–216, May 1996.
[17] S. Majima, K. Kodama, and T. Hasegawa, "Modeling of shape memory alloy actuator and tracking control system with the model," *IEEE Trans. Control Syst. Technol.*, vol. 9, no. 1, pp. 54–59, Jan. 2001.
[18] W. S. Galinaitis, "Two methods for modeling scalar hysteresis and their use in controlling actuators with hysteresis" Ph.D. dissertation, Virginia Polytechnic Inst. State Univ., Blacksburg, VA, 1999.
[19] K. Kuhnen and H. Janocha, "Inverse feedforward controller for complex hysteretic nonlinearities in smart-material systems," *Control Intell. Syst.*, vol. 29, no. 3, pp. 74–83, 2001.
[20] P. Krejci and K. Kuhnen, "Inverse control of systems with hysteresis and creep," *Proc. Inst. Elect. Eng.—Contr. Theory Appl.*, vol. 148, no. 3, pp. 4008–4009, May 2001.
[21] K. Kuhnen and H. Janocha, "Complex hysteresis modeling of a broad class of hysteretic nonlinearities," in *Proc. 8th Int. Conf. New Actuators*, Bremen, Germany, Jun. 2002, pp. 688–691.
[22] R. Koops and G. A. Sawatzky, "New scanning device for scanning tunnel microscope applications," *Rev. Sci. Instrum.*, vol. 63, no. 8, pp. 4008–4009, 1992.
[23] X. Tan and J. S. Baras, "Control of hysteresis in smart actuators, Part I: Modeling, parameter identification, and inverse control," Center for Dynamics and Control of Smart Structures, Cambridge, MA, Tech. Res. Rep. CDCSS TR 2002-8, 2002.
[24] R. C. Smith, Z. Ounaies, and R. Wieman, "A model for rate-dependent hysteresis in piezoceramic materials operating at low frequencies," NASA Langley Research Center, Hampton, VA, Tech. Rep. NASA/CR-2001-211-62, 2001.
[25] W. T. Ang, F. Alija Garmon, P. K. Khosla, and C. N. Riviere, "Modeling rate-dependent hystersis in piezoelectric actuators," in *Proc. IEEE Int. Conf. Intell. Robot. Syst.*, vol. 2, pp. 1975–1980, Oct. 27–31, 2003.
[26] C. N. Riviere, W. T. Ang, and P. K. Khosla, "Toward activetremor canceling in handheld microsurgical instruments," *IEEE Trans. Robot. Autom.*, vol. 19, no. 5, pp. 793–800, Oct. 2003.
[27] R. J. Elble and W. C. Koller, *Tremor*. Baltimore, MD: Johns Hopkins Univ. Press, 1990, p. 1.
[28] S. Charles, "Dexterity enhancement for surgery," in *Computer Integrated Surgery: Technology and Clinical Applications*, R. H. Taylor, S. Lavallée, G. C. Burdea, and R. Mösges, Eds. Cambridge, MA: MIT Press, 1996, pp. 467–471.
[29] C. N. Riviere and P. K. Khosla, "Augmenting the human–machine interface: Improving manual accuracy," in *Proc. IEEE Int. Conf. Robot. Autom.*, Albuquerque, NM, Apr. 20–25, 1997, vol. 4, pp. 3546–3550.

Wei Tech Ang (S'98–M'04) received the B.E. and M.E. degrees in mechanical and production engineering from Nanyang Technological University, Singapore, in 1997 and 1999, respectively, and the Ph.D. degree in robotics from Carnegie Mellon University, Pittsburgh, PA, in 2004.

Since 2004 he has been an Assistant Professor in the School of Mechanical and Aerospace Engineering, Nanyang Technological University. His research interests include medical robotics, mechatronics, mechanism design, kinematics, signal processing, and learning algorithms.

Pradeep K. Khosla (F'95) received the B.Tech. degree from the Indian Institute of Technology, Kharagpur, India, and the M.S. and Ph.D. degrees from Carnegie Mellon University, Pittsburgh, PA, in 1984 and 1986, respectively.

At Carnegie Mellon University, he was an Assistant Professor of electrical and computer engineering and robotics from 1986 to 1990, an Associate Professor from 1990 to 1994, has been Professor since 1994, and was Founding Director of the Institute for Complex Engineering from 1997 to 1999. He is currently the Philip and Marsha Dowd Professor of Engineering and Robotics and Head of the Electrical and Computer Engineering Department. From January 1994 to August 1996 he was a DARPA Program Manager. His research interests include Internet-enabled collaborative design and distributed manufacturing, agent-based architectures for distributed design and embedded control, software composition and reconfigurable software for real-time embedded systems, and reconfigurable and distributed robotic systems. He has authored two books and more than 200 article titles published in various journals, conference papers, and book contributions.

Prof. Khosla was a recipient of the Carnegie Institute of Technology Ladd Award for excellence in research in 1989, the ASEE 1999 George Westinghouse Award for Education, the Siliconindia Leadership Award for Excellence in Academics and Technology in 2000, and the W. Wallace McDowell Award from the IEEE Computer Society in 2001. From 1998 to 2001, he was a Distinguished Lecturer of the IEEE Robotics and Automation Society. He was the General Chairman for the 1990 IEEE International Conference on Systems Engineering, Program Vice Chairman of the 1993 International Conference on Robotics and Automation, General Co-Chairman of the 1995 Intelligent Robotics Systems (IROS) Conference, and Program Vice-Chair for the 1997 IEEE Robotics and Automation Conference. He was a Technical Editor of the IEEE TRANSACTIONS ON ROBOTICS AND AUTOMATION and is currently an Associate Editor of the *ASME Journal of Computers and Information Science in Engineering*.

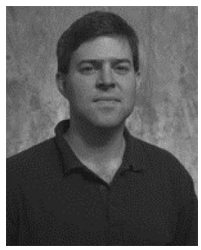

Cameron N. Riviere (S'94–M'96) received the B.S. degrees in aerospace engineering and ocean engineering from Virginia Polytechnic Institute and State University, Blacksburg, in 1989, and the Ph.D. degree in mechanical engineering from The Johns Hopkins University, Baltimore, MD, in 1995.

Since 1995, he has been with the Robotics Institute at Carnegie Mellon University, Pittsburgh, PA, where he is currently an Associate Research Professor. His research interests include medical robotics, control systems, signal processing, learning algorithms, and biomedical applications of human–machine interfaces.